Eur Biophys J (2008) 37:173–182
DOI 10.1007/s00249-007-0213-8

ORIGINAL PAPER

Self-association of adenine-dependent hairpin ribozymes

Yan-Li Li · Marie-Christine Maurel · Christine Ebel · Jacques Vergne · Vitaliy Pipich · Giuseppe Zaccai

Received: 19 March 2007 / Revised: 6 July 2007 / Accepted: 24 July 2007 / Published online: 25 September 2007

Abstract Hairpin ribozymes are flexible molecules that catalyse reversible self-cleavage after the docking of two independently folded internal loops, A and B. The activities, self-association and structures in solution of two 85 base adenine-dependent hairpin ribozymes (ADHR1 and ADHR2) were studied by native gel electrophoresis, analytical centrifugation, and small angle neutron scattering. Bi-molecular RNA interactions such as linear–linear, loop–loop, loop–linear or kissing interactions have been found to be important in the control of various biological functions, and hairpin loops present rich potential for establishing both intra- and intermolecular interactions through standard Watson-Crick base pairing or non-canonical interactions. Similar results were obtained for ADHR1 and ADHR2. At room temperature, they indicated end-to-end self-association of the ribozymes in rod-like structures with a cross-section corresponding to two double strands side-by-side. Dimers, which predominate at low concentration ($\sim$0.1 mg/ml), associate into longer rods, with increasing concentration ($\sim$1 mg/ml). Above 65°C, the dimers and rods dissociated into compact monomers, with a radius of gyration similar to that of tRNA (about 70 bases). The dimers were non-active for catalysis, which suggests that dimer formation, probably by preventing the correct docking of loops A and B, could act as an inhibition mechanism for the regulation of hairpin ribozyme catalysis.

Keywords Neutron scattering · Analytical centrifugation · RNA enzyme dimers

Y.-L. Li · M.-C. Maurel (✉) · J. Vergne
Institut Jacques-Monod, Laboratoire de Biochimie de l'Evolution et Adaptabilité Moléculaire, CNRS, Université Paris VI, Tour 43, 2 place Jussieu, 75251 Paris Cedex 05, France
e-mail: maurel@ijm.jussieu.fr

C. Ebel · G. Zaccai
Institut de Biologie Structurale Jean-Pierre Ebel, CEA, CNRS, Université Joseph Fourier, 41 rue Jules Horowitz, 38027 Grenoble, France

V. Pipich
Institut für Festkörperforschung Forschungszentrum Juelich GmbH, 52425 Juelich, Germany

G. Zaccai
Institut Laue Langevin, 6 rue Jules Horowitz, BP 156X, 38942 Grenoble Cedex 9, France
e-mail: zaccai@ill.fr

Introduction

The RNA world hypothesis in origin of Life theory is supported by the current existence of ribozymes, catalytic RNA molecules with splicing activity involved in rRNA, mRNA maturation and ribosomal RNA that catalyses peptide bond formation (Orgel 1986). At least four kinds of small endonucleolytic ribozymes have been discovered as catalytic motifs within viruses, viroids and satellite RNAs (Symons 1992; Li 2006). These, mainly hairpin and hammerhead motifs, are involved in the replication of small circular RNA species, and perform reversible self-cleavage within viroids and satellite RNAs. The role of small molecules and particularly of some purines in riboswitches (Mandal and Breaker 2004; Serganov et al. 2004) and the fact that most coenzymes are ribonucleotidic cofactors essential to protein activity emphasize another aspect of the modern RNA world, which is somewhat related with ancient pathways. A model proposed for the origin of the transfer RNA molecule (Di Giulio 1992, 2004) suggested that the molecule originated from an RNA hairpin structure, similar to the one proposed by Hopfield (Hopfield

1978), and it has frequently been suggested that RNA hairpin structures might have been involved in some evolutionary stages in the origin of protein synthesis (Di Giulio 2004). Furthermore, dimerization via covalent bonding of similar hairpin structures might have given rise directly to a kind of tRNA molecule (Di Giulio 1992). All these structural features in current RNA molecules could be reminiscent of ancient RNAs.

The hairpin ribozyme is a self cleaving/ligating RNA enzyme first discovered in the minus strand of the satellite RNA associated with tobacco ringspot virus (van Tol et al. 1990). It is composed of two extended helices that are each interrupted by a stretch of non complementary sequence, loops A and B. Juxtaposition of these two loops results in a secondary structure that resembles a hairpin. Extensive mutagenesis and modification interference studies have shown that the essential nucleotides reside in the A and B loops (Berzal-Herranz et al. 1993; Lebruska et al. 2002), and it is possible to reconstitute the catalytic activity in vitro by synthesizing both parts as separate RNAs and mixing them together (Butcher et al. 1995). The nucleolytic ribozyme brings about a self catalyzed site-specific cleavage of the phosphodiester backbone, in loop A, by means of a nucleophilic reaction, in which the adjacent 2′ oxygen atom attacks the 3′phosphorus with departure of the 5′ oxygen, to generate a cyclic 2, 3′ phosphate product and 5′-hydroxyl termini. Catalysis could occur through deprotonation of the 2′-hydroxyl group, facilitation of the trajectory into the in-line transition state, charge stabilization in the transition state, or stabilization of the oxyanion leaving group. It could involve the ribozyme nucleobases as general acid-base catalysts, or be mediated by metal ions in acid–base and/or nucleophilic catalysis. The catalytic mechanisms used by the small self-cleaving ribozymes are still unclear and further structural and functional studies are required.

Ribozymes, like protein enzymes, can exploit more than one catalytic strategy. Each ribozyme adopts a unique structure and follows distinct kinetic and catalytic pathways, as if each motif provided a different evolutionary solution to accomplish the same biological function (Symons 1992). Possible similarities between the reaction mechanisms of the hairpin ribozyme and ribonuclease A have been emphasized (Nesbitt et al. 1997). Although it is difficult to extend this similarity to their catalytic mechanism, it seems likely that the bases G8, A38 and A10 of the ribozyme play the same role in catalysis as the histidine 12, histidine 119, and lysine 41 of ribonuclease A, respectively.

The hairpin ribozyme is a good candidate to test our hypothesis that adenine was a cofactor for early ribozymes. Adenine is a likely prebiotic analog of histidine. Its catalytic capabilities are equivalent to histidine because of the presence of a free imidazole moiety (Maurel and Ninio 1987; Maurel and Décout 1999). It was previously shown that when adenine is placed in a favorable microenvironment its catalytic efficiency is strongly enhanced (Décout 1995; Ricard et al. 1996; Maurel and Décout 1999). Such favorable microenvironments could result from adenine binding to RNA, thereby providing catalytic sites. Hence, the hairpin ribozyme constitutes a good starting point for the search of ribozymes that require catalytic organic cofactors. Starting from inactive hairpin variants, we discovered, by using the systematic evolution of ligands by the exponential enrichment (SELEX) method, two new hairpin ribozymes (ADHR1 and ADHR2) that require adenine as catalytic cofactor for their reversible self-cleavage (Meli et al. 2003) (Fig. 1).

Bi-molecular RNA interactions including linear–linear, loop–loop and loop–linear pairing are important in the control of various functions (Craig et al. 1971). Loop–loop interactions are frequently used to trigger initial recognition between two RNA molecules. Hairpin loops can base pair via their complementary sequences to form a so-called kissing interaction (Beaurain et al. 2003), found in tRNAs (Quigley and Rich 1976; Wagner and Simons 1994), natural antisense RNAs (Zeiler and Simons 1998), and within peripheral components of subgroup IC1 and ID introns (Lehnert et al. 1999). More recently the kissing interaction was shown to be crucial for the folding and activity of the

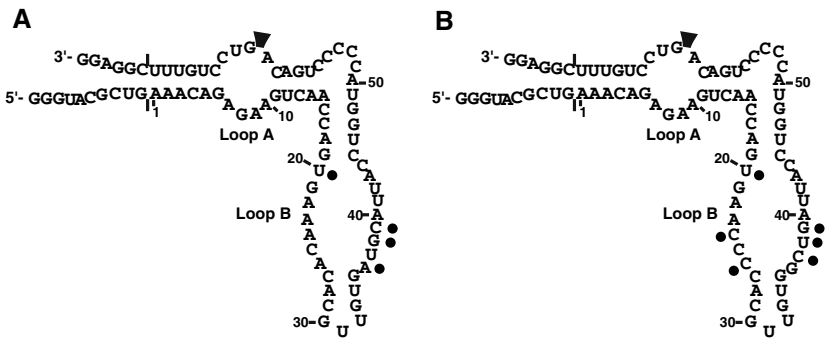

Fig. 1 **a** ADHR1 structure. **b** ADHR2 structure. The cleavage site is indicated with an *arrowhead.* Nucleotides that changed with respect to the wild-type hairpin ribozyme are indicated with *black circles*. Bases are numbered according to the wild-type hairpin ribozyme. (Meli et al. 2003)

Neurospora varkud satellite ribozyme (Hiley and Collins 2001). Recent work on the folding dynamics of complex, biologically active RNA molecules indicate that folding occurs in a hierarchical manner over a large range of time scales (Brion and Westhof 1997). Long-range tertiary interactions are responsible for critical steps to stabilize the final, fully compacted, biologically active structures of RNA molecules (Jaeger et al. 2001). In the case of the "kissing" hairpin complex of the HIV TAR hairpin loop and its complement, the alternation helical twist pattern, plus other distortions in the loop–loop helix seems to be important for their recognition (Chang and Tinoco 1997). Furthermore, the in vitro folding study of hammerhead ribozyme showed that, the kissing-loop interactions of two RNA molecules can favour, in vivo, the adoption and stabilization of a compact fold critical for viroid viability (Gago 2005).

In December 2006, there were one hundred and eleven ribozyme related high resolution structures in the protein data bank, solved by X-ray diffraction, NMR and fluorescence transfer (http://www.rcsb.org/pdb/). Structures obtained from small angle X-ray or neutron scattering (SAXS, SANS) are at low resolution. These experimental methods, however, have the significant advantage of providing information on over-all molecular conformation or shape and quaternary structure as a function of solvent conditions and temperature. Furthermore, SAS data are easily obtained on an absolute scale, which permits the measurement of the molar masses of the scattering particles as well as of their conformations. In contrast to methods such as gel filtration, which measure a single parameter related to the diffusion coefficient and cannot distinguish between an elongated shape or larger mass, for example, SAS provides separate and independent information on particle mass and shape. RNA structures, in particular, are sensitive to external conditions, and have profited from SAS studies (Li et al. 1983; Zaccai and Xian 1988). In the current study, we followed cleavage kinetics, and measured conformations and self-association of the two-adenine dependent hairpin ribozymes, under various temperature conditions. Results were similar for the two molecules, ADHR1 and ADHR2.

Materials and methods

RNA preparation of ADHR1, ADHR2 and their mutants

The 85-nucleotide-long templates are single-stranded DNA (Meli et al. 2003). The entire sequence for ADHR1 is 5′CCTCCGAAACAGGACTGTCAGGGGGTACCAGGTAATGCATCACAACGTGTGTTTCACTGGTTGACTTCTCTGTTTCAGCGTACCC-3′; and 5′-CCTCCGAAACAGGACTGTCAGGGGGTACCAGGTAATCAGCCACAACGTGGGGTTCACTGGTTGACTTCTCTGTTTCAGCGTACCC-3′ for ADHR2. For two mutants of ADHR1, the entire sequence is 5′-CCTCCGAAACAGGACTGTCAGGGGGTACCAGGTAATGCATCAC**TTT**GTGTGTTTCACTGGTTGACTTCTCTGTTTCAGCGTACCC-3′ for ADHR1 first mutant, and 5′-CCTCCGAAACAGGACTGTCA**TTTTT**TACCAGGTAATGCATCACAACGTGTGTTTCACTGGTTGACTTCTCTGTTTCAGCGTACCC-3′ for ADHR1 Mut2. For two mutants of ADHR2, their sequences are the following: 5′-CCTCCGAAACAGGACTGTCAGGGGGTACCAGGTAATCAGCCAC**TTT**GTGGGGTTACTGGTTGACTTCTCTGTTTCAGCGTACCC-3′ for ADHR2 Mut1, and 5′-CCTCCGAAACAGGACTGTCA**TTTTT**TACCAGGTAATCAGCCACAACGTGGGGTTACTGGTTGACTTCTCTGTTTCAGCGTACCC-3′ for ADHR2 Mut2 (Mutated nucleotides are in bold). The two primer binding regions are located in the 5′- and 3′- termini. Two primers were synthesized chemically (Sigma-Proligo). The sequence of primer P1 (promoter primer) is 5′-**TAATACGACTCACTATA**GGGTACGCTGAAACAGA-3′ (T7 promoter sequence in bold), and that of primer P2 is 5′-CCTCCGAAACAGGACTGTCAGGGGGTACCAG-3′.

A 4-ml PCR (Invitrogen) reaction with 1 μM each primer and 0.016 μM template amplified with 10 cycles. The double-stranded DNAs were then ethanol-precipitated and submitted to in vitro transcription (4 ml) using T7 RNA polymerase (Fermentas). The reaction mixture contained 2.5 mM each rNTP, transcription buffer (Fermentas), 0.15 μM DNA and 2,400 units of T7 RNA polymerase. After overnight incubation at 37°C, and a treatment by DNAse (2 units/1 μg DNA), followed by deproteinization and ethanol precipitation, the transcription product was purified on a 10% denaturing polyacrylamide gel (PAGE), ethanol-precipitated, and resuspended in distilled water.

Cleavage reaction of ADHR1, ADHR2 and their mutants on native gel

Transcribed RNAs were dissolved in cleavage buffer (40 mM HEPES, 6 mM $MgCl_2$, with or without 50 mM NaCl, pH 7.5). The solutions were then incubated with 1/9 volume of cleavage buffer alone (negative controls) or with 1/9 volume of adenine containing cleavage buffer (4 mM adenine). Aliquots were removed from the mixtures at various times and reactions were stopped by freezing. The reactions were analyzed by native PAGE and ethidium bromide staining. RNA uncleaved and fragments were revealed by UV trans-illumination and quantified using an NIH image analyzer, according to the percentage of dimer formation and that of cleavage were calculated.

Small angle neutron scattering

Experiments were performed at the KWS-1 SANS camera at the Forschungszentrun, Juelich, Germany (http://www.fz-juelich.de/iff/wns_kws1/) and the D22 SANS camera at the Institut Laue Langevin, Grenoble, France (http://www.ill.fr/YellowBook/D22/). On both instruments, sample intensities were recorded with neutrons of λ = 7 Å wavelength (20% $\Delta\lambda/\lambda$ for KWS-1, 10%, for D22). The scattering data were corrected for background, efficiency of the detector cells, then radially averaged around the direct beam centre and calibrated in absolute units by a Lupolen secondary standard for KWS-1, and 1.00 mm of H_2O for D22. The scattered neutron intensity was determined as the macroscopic cross-section I(Q) in units of (cm^{-1}) versus the momentum transfer $Q = (4\pi/\lambda)\sin\theta$ where 2θ is the scattering angle. On KWS-1, the scattering experiments were performed for 2 and 4 m detector to sample distance and corresponding collimation distance operational modes covering a scattering vector amplitude range of $0.011 < Q$ ($Å^{-1}$) < 0.17. On D22, The sample to detector distance was 3 m, with 4 m collimation; the detector was off-set laterally with respect to the beam to provide a Q range of $0.0126 < Q$ ($Å^{-1}$) < 0.267. Sample volumes of about 150 µl were contained in 1.00 mm pathlength quartz cells. In a first step of data treatment, the scattering from the empty cell was subtracted from the merged intensities of each RNA or buffer sample, appropriately corrected for transmission. The buffer scattering was then subtracted from that of each sample, and the quality of the subtraction was verified by inspection of the resulting corrected intensities at high Q-values. Analysis in terms of molecular structures was performed on the calibrated and buffer subtracted data.

Analytical ultra-centrifugation (AUC)

Sedimentation velocity experiments of ADHR1 and ADHR2 RNA were performed at 20°C and 42,000 or 45,000 rpm, using a XLI Beckman ultracentrifuge with the AnTi-60 rotor and 3 or 12 mm two-channel centrepieces. The sedimentation profiles were obtained for 3 h and 45 min every 10 min at 260 nm. Analysis was performed with the program Sedfit—available free at http://www.analyticalultracentrifugation.com—which allows obtaining continuous distributions $c(s)$ of sedimentation coefficients, s (Schuck 2000). For the analysis and derivation of $s_{20,w}$ values, we took tabulated solvent density and viscosity and an RNA partial specific volume of 0.58 cm^3/g (Durchschlag 1986).

Molecular masses and radii of gyration

The radii of gyration of scattering contrast, R_g, of the samples were determined from the scattered intensity, $I(Q)$ by applying the Guinier approximation, which is valid for a Q range in which $(R_gQ)^2 \sim 1$ (Jacrot 1976)

$$I(Q) = I(0)\exp\left(-R_g^2Q^2/3\right). \quad (1)$$

The molar mass (M) for each sample was extracted from the absolute scale value of $I(0)$ by using Eq. (2) (Jacrot and Zaccai 1981).

$$\frac{I(0)}{c} = \frac{10^{-3}}{N_A}\left(N_A\frac{\sum b - \rho^0 V}{M}\right)^2 M. \quad (2)$$

The factor 10^{-3} is required in order to express RNA concentration c (determined from OD at 260 nm) in the usual way in mg/ml, N_A is Avogadro's number, the term in brackets is the excess scattering length of the RNA per unit molar mass (Σb is the scattering length sum of RNA atoms, calculated from its composition. ρ^0 is scattering length density of the solvent, V is RNA volume calculated from its partial specific volume), and M is RNA molar mass in grams per mole.

In the case of a rod-like particle in which one dimension is significantly larger than the other Eq. (3) is a good approximation that yields the cross-sectional radius of gyration, R_c (Porod 1982):

$$I(Q)Q = A\exp\left(-R_c^2Q^2/2\right). \quad (3)$$

The molar mass per unit length (M/L) of the rod is calculated from A, the value of the function extrapolated to $Q = 0$, by using Eq. (4)

$$\frac{A}{c} = \pi\frac{10^{-3}}{N_A}\left(N_A\frac{\sum b - \rho^0 V}{M}\right)^2\frac{M}{L}. \quad (4)$$

Similarly to the radius of gyration of a body being equal to the distribution of mass equivalent (contrast in the case of scattering experiments) weighted by the square of its distance to the centre of mass equivalent, the cross sectional radius of gyration corresponds to the distribution in the cross section of a long rod projected on a two dimensional plane perpendicular to the axis of the rod. From these relations, the radius of gyration of a homogeneous sphere of radius R is calculated to be $\sqrt{(3/5)}$ R; The cross-sectional radius of gyration of a homogeneous rod of circular cross-section of radius R is equal to the two dimensional radius of gyration of a filled circle, and is calculated to be $\sqrt{(1/2)}$ R.

If the sample is polydisperse, the $I(0)$ and R_g^2 values represent number averages:

$$I(0) = \sum_j N_j I_j(0) \quad (5)$$

$$R_g^2 = \sum_j \frac{N_j R_{gj}^2 I_j(0)}{I(0)} \quad (6)$$

where N_j is the number of particles j in the solution with radius of gyration R_{gj}, and forward scattered intensity value $I_j(0)$.

Results

Similar results were obtained for both ribozymes.

AUC results

Sedimentation velocity AUC is a key technique for the characterisation of sample homogeneity and equilibrium macromolecular association (Ebel 2007). ADHR1 ribozyme at three concentrations in the range 0.01–0.1 mg/ml appeared as mixtures of mainly monomers and dimers with some higher aggregates depending on concentration. A typical set of fitted sedimentation profiles and residuals is shown in Fig. 2a and b, respectively, indicating the good quality of the data and fit. The sedimentation coefficient distribution, expressed in units of absorbance at 260 nm for a 1.00 cm path-length is plotted in Fig. 2c for the three concentrations. Samples are clearly not monodisperse; the proportion of the different species depending on concentration suggests equilibrium auto-association. The positions of the first two maxima do not vary significantly, which corresponds to slow association–dissociation. The low signal corresponding to the largest species prohibits an unambiguous interpretation of the shift in the position of the largest particle, from nearly 9.5S to 11S, for concentrations of ADHR1 of 0.041 and 0.116 mg/ml. It may correspond to an artefact in data analysis or to equilibrium between species. In Fig. 2d, we plotted published log s_{20w} versus log (number of bases) for several unfolded (in absence of Mg^{2+}) RNA molecules (values from Serdyuk 2007). Note that they are well fitted by a straight line with a gradient of 0.47. A hypothetical curve corresponding to compact globular particles with frictional ratio of 1.25 is also plotted. The figure shows the experimental points for ADHR1 (s_{20w} of 4.3S, 6.5S, 10 ± 1S), assuming the peaks correspond to monomer (85 bases), dimer and tetramer, respectively. The points for the 4.3S and 6.5S particles lie between the two curves, confirming the monomer and dimer association state and their intermediate shapes (ADHR is expected to have a more compact shape than if unfolded). The position of the broad peak at about 10 ± 1S

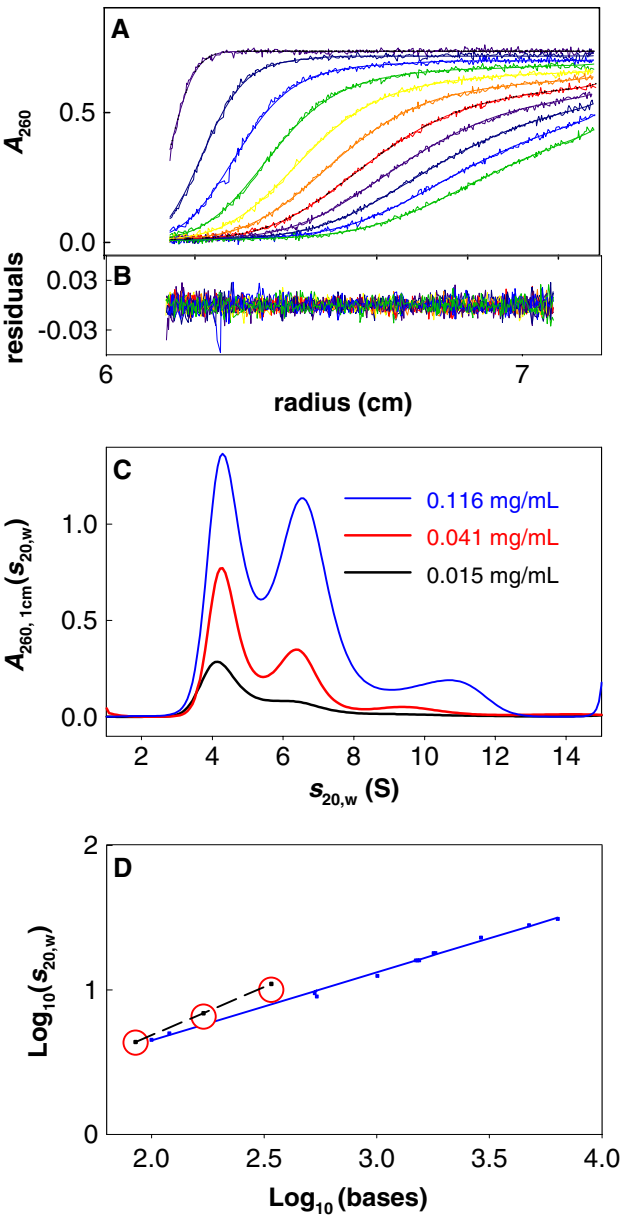

Fig. 2 Sedimentation velocity of ADHR1 at various concentrations in 5 mM MgCl2, 150 mM KCl, 0.1 mM EDTA, 10 mM MOPS pH 7. **a** Superimposition of selected fitted experimental profiles obtained at 20°C for ADHR2 in the **b** residuals of the fit in (**a**). **c** Sedimentation coefficient distribution, in units of absorbance at 260 nm for a 1.00 cm path-length, for the indicated concentrations. **d** Log $s_{20\,w}$ versus Log (number of bases) for a set of extended (in absence of Mg^{2+}) RNA molecules (Serdyuk et al. 2007) (*blue squares*). The fitted straight line has a gradient of 0.47. The *black squares* and *dashed black line* gives calculated *s*-values with a frictional ratio of 1.25 for globular compact species. The data points (*open circles*) at $s_{20\,w}$ values of 4.3S, 6.5S, 10 ± 1S were plotted against values for ADHR1 monomer (85 bases), dimer and tetramer, respectively. The size of the *circles* corresponds to the error bar on the 10S peak

corresponds reasonably to a tetramer, while it may contain contributions from higher aggregates. This *s*-value cannot correspond to a trimer, for which a value in the 6.9–9.1 range would have been expected. A trimer could be present at the intermediate concentration of 0.04 mg/ml. Our data do not contain enough information to ascertain or exclude the possibility of a transient trimer.

Similar experiments on ADHR2 and ADHR1 at 0.02 mg/ml in the presence or absence of NaCl gave similar results. The reason for which the $c(s)$ curves do not have the same resolution in this series of experiments in the presence or absence of salt were not elucidated. It could be related for example to different kinetics of inter-conversion between the species (Fig. 3).

Neutron scattering results

At room temperature (25°C) and concentrations close to 2 mg/ml in 6 mM $MgCl_2$, HEPES 40 mM, pH 7.5: Guinier analysis (Fig. 4a, Eq. 1) gave a radius of gyration of 47 ± 1 Å and a molar mass calculated from $I(0)$ by using Eq. (2) of 84,000 g/mole.

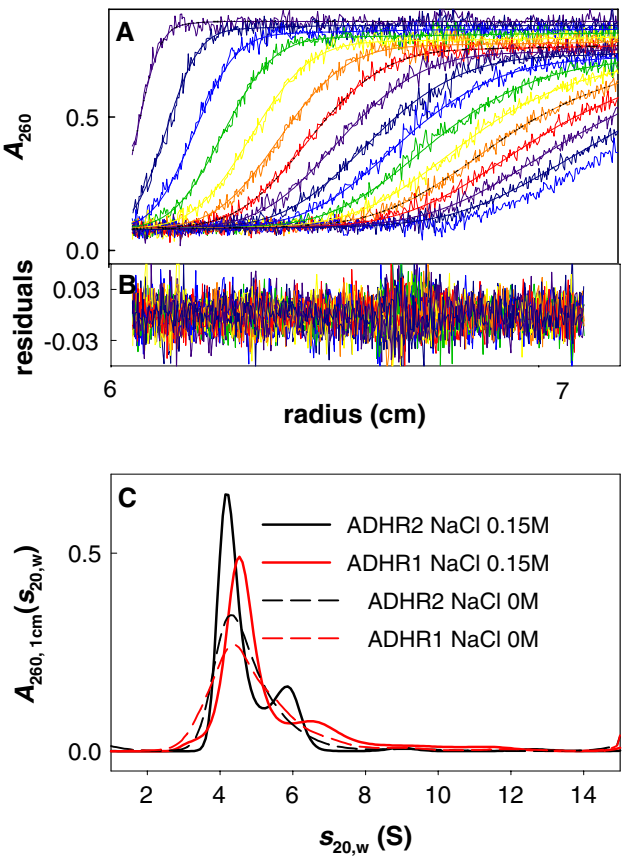

Fig. 3 Sedimentation velocity of ADHR1 and ADHR 2 at 0.02 mg/ml in 6 mM $MgCl_2$, 40 mM Hepes pH 7, in the absence or presence of NaCl 150 mM. **a** Superimposition of selected fitted experimental profiles obtained at 20°C for ADHR 2 in the presence of salt. **b** Residuals of the fit in (**a**). **c** Sedimentation coefficient distributions, in units of absorbance at 260 nm, for the indicated samples. Concentration calculated from A_{260}varies between 0.018 and 0.020 mg/ml

The scattering curve is consistent with that of long rod-like particles. Data analysis using Eqs. (3) and (4) (Fig. 4b) yielded a cross-sectional radius of gyration of 11.7 ± 0.2 Å and mass per unit length of 470 g/mole/Å.

The molar mass of the ribozymes is 27,200 g/mole. The AUC, Guinier and rod approximation parameters interpreted in terms of polydispersity (Eqs. 5, 6) indicate that the ribozymes, self associate to form elongated particles. Inspired by the AUC results, the number average molar mass of 84,000 g/mole indicates the presence of monomers, and higher aggregates, in these conditions. Figure 4b, however, clearly suggests that the cross-section of the particles is close to monodisperse so that aggregation is along the length of the rod. From Eqs. (3), (4), assuming a cylindrical rod model, the particles have a cross-sectional radius of 16 Å and a mass per length corresponding on average to 2 base pairs side by side in approximate A-RNA conformation (about 3 Å rise between adjacent bp). Note that the radius of a homogeneous circle is equal to $\sqrt{2}\,R_c$; two base pairs side by side fit in a circle of radius slightly larger than 20 Å, which suggests a more compact "sideways" arrangement. The length of the number average rod was calculated to be about 160 Å from the average radius of gyration of 47 Å and R_c value

$$R_g^2 = R_c^2 + \frac{1}{12}L^2. \tag{7}$$

Two extreme models can be proposed for the dimer and higher aggregates, with similar cross-sections: two elongated approximately single helix molecules side by side; a more compact hairpin molecule with the two helices side by side, associated end to end with another one. Considering that the data are strongly in favour of association along the length of the rod, the second model is the more likely one.

Addition of 0.4 mM adenine co-factor to the samples in the same temperature and buffer conditions led to a small and probably insignificant change in the scattering curve (Fig. 4c); the radius of gyration was 50 ± 1 Å, for an average molar mass of 80,000 g/mole. The results showed either that the ribozymes in their various associated forms maintained essentially intact and unchanged conformations upon self-cleavage, or that the dimer and higher aggregate populations, which dominate the scattering, were inactive and self-cleavage did not take place.

After the reaction, the mixture was heated to 90°C to improve the dissociation of RNA fragments. The SANS of the ribozyme plus adenine samples was performed at 65°C (the highest temperature then attainable on the sample holder device). The scattering curves changed drastically to

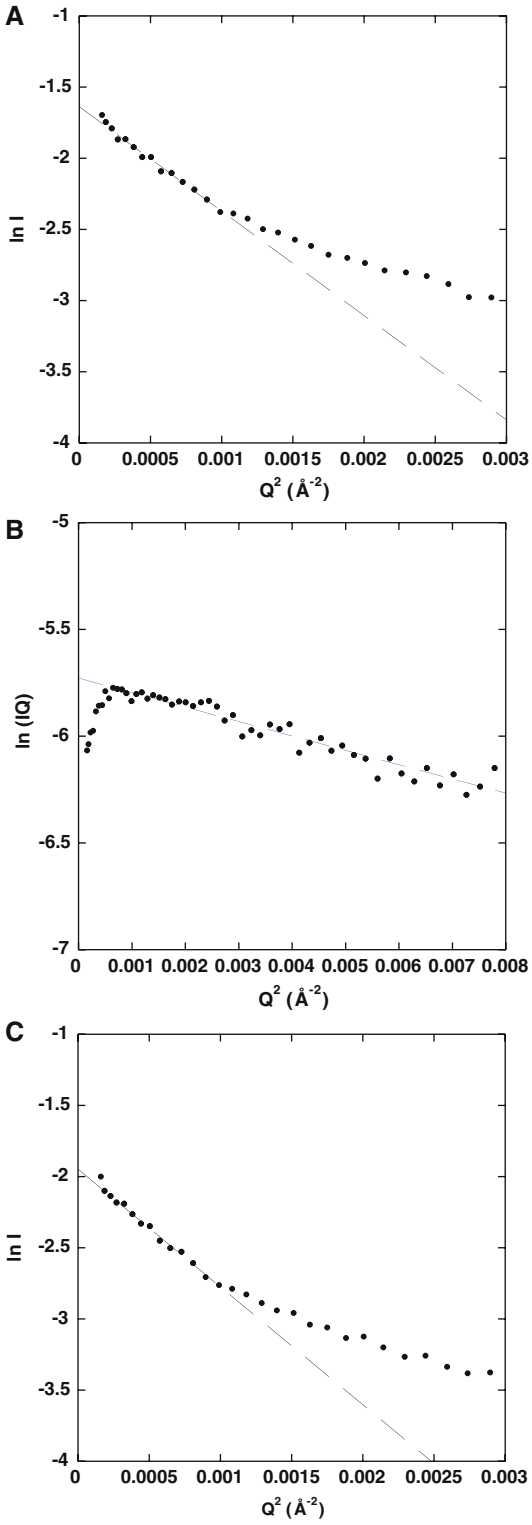

◀ **Fig. 4** Neutron scattering curves at room temperature for ADHR1 at a concentration close to 2 mg/ml, in 6 mM $MgCl_2$, HEPES 40 mM, pH 7.5. **a** Guinier plot giving a radius of gyration of 47 ± 1 Å, and a molar mass of 84,000 g/mole; the fit range corresponds to $0.59 < QR_G < 1.33$. **b** The rod approximation plot for the same sample yielding a cross-sectional radius of gyration of 11.7 ± 0.2 Å and mass per unit length of 470 g/mole/Å. The fit range is for $0.28 < QR_C < 1.03$. **c** Guinier plot after addition of 0.4 mM adenine co-factor to the sample in the same temperature and buffer conditions as above. The radius of gyration is 50 ± 1 Å, for an average molar mass of 80,000 g/mole; the fit range is for $0.63 < QR_G < 1.43$

indicate solutions with a particle radius of gyration of 26 ± 0.5 Å (Fig. 5a). After correction of the concentration for the known fraction of RNA degradation due to the temperature, a particle molar mass of 27,000 g/mole was calculated by using Eq. (2). The radius of gyration and molar mass values showed that the rod shaped particles had dissociated into monomers, in the solvent conditions and temperature conditions. For comparison, yeast transfer RNA^{phe} with an anion molar mass of 24,500 g/mole has a radius of gyration of 23 Å, if calculated from the crystal structure or measured in solution in NaCl or KCl (Li et al. 1983; Zaccai and Xian 1988), indicating that the hairpin monomer has a slightly less compact shape than that of tRNA.

Finally, after heating to 90°C, ADHR was measured at 65°C in the absence of adenine (Fig. 5b). For this sample also, the monomer was clearly observed with a radius of gyration of 24 ± 1 Å and a measured molar mass of 28,000 g/mole. The absolute scale molar mass values measured for the "with" and "without" adenine co-factor experiments suggest that the cleaved but non-degraded RNA molecules do not separate into two distinct fragments even upon incubation at high temperature. This is not a strong conclusion, however, because of the uncertainty in the concentration correction for the fraction of RNA degradation due to the high temperature, estimated from gel experiments.

Model building

A geometrical rod model of hairpins associating end to end, can be fitted in terms of the monomer structure observed at high temperature. Clearly, the monomer conformation is in agreement with such a model, only provided of course that there is no major conformational change between the high temperature and the self-associated states. The orientation of protomers within the rod and interactions between them can be discussed in terms of the "kissing" type interactions or using work such as described by Jaeger et al. (2001). Various ways of achieving the association process are through a linear–loop interaction, in which the recognition occurs between 5′ single-stranded and the little loop at the end of loop B, or by a linear–bulge interaction, in which the 5′ single-strand recognizes the unpaired junction sequence situated between loops A and B, or by kissing interactions between two ends of loop B from two individual molecules (Fig. 6).

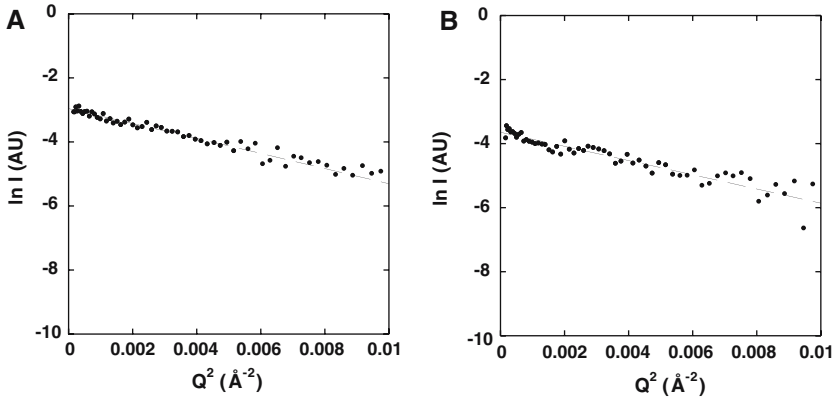

Fig. 5 Neutron scattering curves of ADHR1 at high temperature in the same buffer as for Fig. 3. **a** Guinier plot for the ribozyme plus adenine sample described in Fig. 3c, after incubation at 90°C, and measured at 65°C. The radius of gyration is 26 ± 0.5 Å, and the molar mass is 27,000 g/mole (see text for the concentration determination); the fit range is $0.39 < QR_G < 1.91$. **b** Guinier plot for a fresh ADHR1 sample in absence of adenine, measured at 65°C after heating to 90°C. The radius of gyration is 24 ± 1 Å for a measured molar mass of 28,000 g/mole; the fit range is for $0.72 < QR_G < 1.76$

The molecules' dimerization was verified by electrophoresis on native gels, with which RNAs of different conformations or lengths can be distinguished (Fig. 7). The kinetics of self-cleavage for the two ribozymes was also controlled by the same method. The measurements indicated that the dimers were inert, and that only the monomer was catalytically active. Higher aggregates were not observed on the gels at these RNA concentrations.

Mutagenesis assay

In order to test the different dimer models presented in Fig. 6, we mutated in the small terminal loop (Mut1) that would affect the formation of the linear–loop structure, or the "kissing" type interactions; and mutated the unpaired junction sequence (Mut2) between loop A and loop B that would affect the linear–bulge interaction. Kinetics of the two ribozymes and their mutants were observed on native gels (Fig. 7). Cleavage was carried out under the same conditions as that for neutron scattering experiments, in the presence of 40 mM HEPES, 6 mM $MgCl_2$, with or without 0.4 mM adenine, pH 7.5. On native gel, ADHR1, ADHR2 and their mutants, ADHR1 Mut1, ADHR1 Mut2, ADHR2 Mut1 and ADHR2 Mut2, formed dimers from the beginning of the reaction. For all the mutants, the percentage of dimer formation decreased, this diminution is more important for Mut2 than that for Mut1 (Fig. 7). The

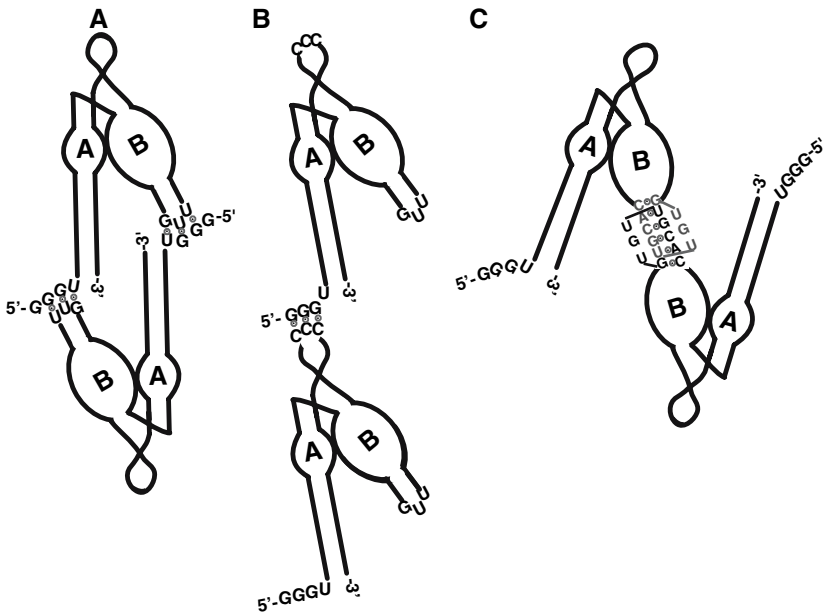

Fig. 6 Schematic models of ADHR1/ADHR2 dimerization of. **a** Linear/loop interaction. Three nucleotides 'GUU' at the end of loop B were replaced by 'AAA' for the mutagenesis experiment, Mut1. **b** Linear/bulge interaction. Three nucleotides 'CCC' in the bulge between loop A and loop B were replaced with 'AAA' for the mutagenesis experiment, Mut2. **c** 'Kissing' type interaction of ADHR1/ADHR2

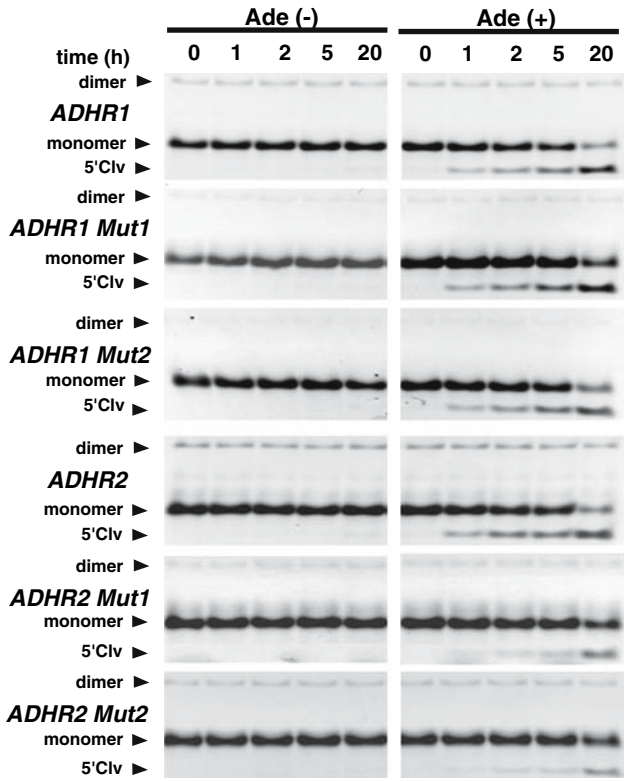

Fig. 7 Native gel electrophoresis analysis of cleavage kinetics for ADHR1, ADHR2 and their mutants, ADHR1Mut1, ADHR1Mut2, ADHR2Mut1 and ADHR2Mut2. In presence (Ade (+)) or absence (Ade (–)) of adenine, respectively. 5'Clv: 5' cleaved product

intensity of dimers was not influenced by time of cleavage incubation. On the contrary, cleavage efficiency increased proportionally with the diminution of the monomer portion.

Discussion

Loop–linear interactions occur between loops and short single-stranded sequences, in numerous cases as between tRNAs and their complementary trinucleotide codons (Jaskunas et al. 1968; Eisinger 1971), or natural antisense RNAs that bind to complementary regions on specific target RNAs to control their biological function (Wagner and Simons 1994).

In this work, we demonstrated using SANS from solution that two adenine-dependent hairpin ribozymes, ADHR1 and ADHR2, with a monomeric structure similar to tRNA associate end to end into rod like structures, including dimers and higher aggregates. From AUC sedimentation velocity experiments, the association appeared to be a concentration dependent equilibrium. The SANS data collected at about 2 mg/ml showed the rods to have an average length of about 160 Å with a cross-sectional radius and mass per unit length consistent to two side by side base pairs in A-RNA conformation. This type of association may be accounted for by a loop-linear reaction, in which the recognition occurred between the 5′ end single strand and the extremity of loop B, or the bulge junction between loop A and loop B. It may be also a "kissing" type reaction between two ends of loop B from two individual molecules. Tetramers could form through a combination of the "kissing" model and a bulge–linear interaction (Fig. 6). The role played by these interactions was supported by mutagenesis experiments, which showed that dimer formation was affected after the replacement of the nucleotides that were supposed to be important for association. Electrophoresis on native gels experiments showed that the dimers were inactive; suggesting the dimerization process could be a negative regulation of the ribozyme function, which could be "employed" by viroids to temporize their replicative progeny in the host cells.

Acknowledgments Y.-L. L was supported by fellowships from the "Association pour l'Information et la Recherche en Oncologie" and from the "Fondation des Treilles". We are grateful to the Neutron and Muon Integrated Infrastructure Initiative NMI3 of the EU for travel grants to perform the experiments and to the staff of ILL and Juelich research centres for support.

References

Beaurain F, Di Primo C, Toulme JJ, Laguerre M (2003) Molecular dynamics reveals the stabilizing role of loop closing residues in kissing interactions: comparison between TAR-TAR* and TAR-aptamer. Nucleic Acids Res 31:4275–4284

Berzal-Herranz A, Joseph S, Chowrira BM, Butcher SE, Burke JM (1993) Essential nucleotide sequences and secondary structure elements of the hairpin ribozyme. EMBO J 12:2567–2573

Brion P, Westhof E (1997) Hierarchy and dynamics of RNA folding. Annu Rev Biophys Biomol Struct 26:113–137

Butcher SE, Heckman JE, Burke JM (1995) Reconstitution of hairpin ribozyme activity following separation of functional domains. J Biol Chem 270:29648–29651

Chang KY, Tinoco I Jr (1997) The structure of an RNA "kissing" hairpin complex of the HIV TAR hairpin loop and its complement. J Mol Biol 269:52–66

Craig ME, Crothers DM, Doty P (1971) Relaxation kinetics of dimer formation by self complementary oligonucleotides. J Mol Biol 62:383–401

Décout JL, Vergne J, Maurel MC (1995) Synthesis and catalytic activity of adenine containing polyamines. Macromol Chem Phys 196:2615–2624

Di Giulio M (1992) On the origin of the transfer RNA molecule. J Theor Biol 159:199–214

Di Giulio M (2004) The origin of the tRNA molecule: implications for the origin of protein synthesis. J Theor Biol 226:89–93

Durchschlag H (1986) Specific volumes of biological macromolecules and some other molecules of biological interest. In: Hinz HJ (ed) Thermodynamic data for biochemistry and biotechnology. Springer, New York, pp 45–128

Ebel C (2007) Analytical ultracentrifugation. State of the art and perspectives. In: Uversky V, Permyakov EA (eds) Protein structures: methods in protein structure and stability analysis. Nova Science Publishers, New York

Eisinger J (1971) Complex formation between transfer RNA's with complementary anticodons. Biochem Biophys Res Commun 43:854–861

Gago S, De la Pena M, Flores R (2005) A kissing-loop interaction in a hammerhead viroid RNA critical for its in vitro folding and in vivo viability. RNA 11:1073–1083

Hiley SL, Collins RA (2001) Rapid formation of a solvent-inaccessible core in the *Neurospora* Varkud satellite ribozyme. EMBO J 20:5461–5469

Hopfield JJ (1978) Origin of the genetic code: a testable hypothesis based on tRNA structure, sequence, and kinetic proofreading. Proc Natl Acad Sci USA 75:4334–4338

Jacrot B (1976) Neutron scattering in biology. Rep Prog Phys 39:911–953

Jacrot B, Zaccai G (1981) Determination of molecular weight by neutron scattering. Biopolymers 20:2414–2426

Jaeger L, Westhof E, Leontis NB (2001) TectoRNA: modular assembly units for the construction of RNA nano-objects. Nucleic Acids Res 29:455–463

Jaskunas SR, Cantor CR, Tinoco I Jr (1968) Association of complementary oligoribonucleotides in aqueous solution. Biochemistry 7:3164–3178

Lebruska LL, Kuzmine II, Fedor MJ (2002) Rescue of an abasic hairpin ribozyme by cationic nucleobases: evidence for a novel mechanism of RNA catalysis. Chem Biol 9:465–473

Lehnert K, Ni J, Leung E, Gough S, Morris CM, Liu D, Wang SX, Langley R, Krissansen GW (1999) The integrin alpha10 subunit: expression pattern, partial gene structure, and chromosomal localization. Cytogenet Cell Genet 87:238–244

Li ZQ, Giege R, Jacrot B, Oberthur R, Thierry JC, Zaccai G (1983) Structure of phenylalanine-accepting transfer ribonucleic acid and of its environment in aqueous solvents with different salts. Biochemistry 22:4380–4388

Li YL, Tobé S, Chabauty A, Maurel MC (2006) From ancient to modern RNA world: a metabolic story. In: Sharma (ed) Plant genome: biodiversity and evolution, vol. 2. Science Publishers, Enfield, pp 1–38

Mandal M, Breaker RR (2004) Adenine riboswitches and gene activation by disruption of a transcription terminator. Nat Struct Mol Biol 11:29–35

Maurel MC, Décout JL (1999) Origins of life: molecular foundations and new approaches. Tetrahedron 55:3141–3182

Maurel MC, Ninio J (1987) Catalysis by a prebiotic nucleotide analog of histidine. Biochimie 69:551–553

Meli M, Vergne J, Maurel MC (2003) In vitro selection of adenine-dependent hairpin ribozymes. J Biol Chem 278:9835–9842

Nesbitt S, Hegg LA, Fedor MJ (1997) An unusual pH-independent and metal-ion-independent mechanism for hairpin ribozyme catalysis. Chem Biol 4:619–630

Orgel LE (1986) RNA catalysis and the origins of life. J Theor Biol 123:127–149

Porod G (1982) Small Angle Scattering, chap 2. In: Glatter O, Kratky O (eds) Academic, London

Quigley GJ, Rich A (1976) Structural domains of transfer RNA molecules. Science 194:796–806

Ricard J, Vergne J, Decout JL, Maurel MC (1996) The origin of kinetic cooperativity in prebiotic catalysts. J Mol Evol 43:315–325

Schuck P (2000) Size-distribution analysis of macromolecules by sedimentation velocity ultracentrifugation and Lamm equation modeling. Biophys J 78:1606–1619

Serdyuk IN, Zaccai NR, Zaccai J (2007) Methods in molecular biophysics: structure, dynamics, function. Cambridge University Press, Cambridge

Serganov A, Yuan YR, Pikovskaya O, Polonskaia A, Malinina L, Phan AT, Hobartner C, Micura R, Breaker RR, Patel DJ (2004) Structural basis for discriminative regulation of gene expression by adenine- and guanine-sensing mRNAs. Chem Biol 11:1729–1741

Symons RH (1992) Small catalytic RNAs. Annu Rev Biochem 61:641–671

van Tol H, Buzayan JM, Feldstein PA, Eckstein F, Bruening G (1990) Two autolytic processing reactions of a satellite RNA proceed with inversion of configuration. Nucleic Acids Res 18:1971–1975

Wagner EG, Simons RW (1994) Antisense RNA control in bacteria, phages, and plasmids. Annu Rev Microbiol 48:713–742

Zaccai G, Xian SY (1988) Structure of phenylalanine-accepting transfer ribonucleic acid and of its environment in aqueous solvents with different salts. Biochemistry 27:1316–1320

Zeiler BN, Simons RW (1998) Antisense RNA structure and function. In: Simons RW, Grunberg-Manago M (eds) RNA structure and function, Cold Spring Harbor Laboratory Press, Cold Spring Harbor, pp 437–464